Effect of rotation on the translational and vibrational energy dependence of the dissociative adsorption of D_2 on Cu(111)

H. A. Michelsen,[a] C. T. Rettner, and D. J. Auerbach
IBM Research Division, Almaden Research Center, 650 Harry Road, San Jose, California 95120-6099

R. N. Zare
Department of Chemistry, Stanford University, Stanford, California 94305

(Received 6 November 1992; accepted 8 February 1993)

We have investigated the dependence on the rotational and vibrational states of the translational energy of $D_2(v,J)$ formed in recombinative desorption from Cu(111). These results provide information about the effect of rotational energy relative to that of vibrational and translational energy on the dissociative chemisorption of D_2 on Cu(111). The range of rovibrational states measured includes rotational states $J=0$–14 for vibrational state $v=0$, $J=0$–12 for $v=1$, and $J=0$–8 for $v=2$. D_2 molecules were detected in a quantum-state-specific manner using three-photon resonance-enhanced multiphoton ionization (2+1 REMPI). Kinetic energies of desorbed molecules were obtained by measuring the flight time of D_2^+ ions in a field-free region. The mean kinetic energies determined from these measurements depend strongly on the rotational and vibrational states. Analyzing these results using the principle of detailed balance confirms previous observations that vibrational energy is effective, though not as effective as translational energy, in promoting adsorption. Rotational motion is found to hinder adsorption for low rotational states ($J<5$) and enhance adsorption for high rotational states ($J>5$). Even for high J states, however, rotational energy is less effective than either vibrational energy, which is 30%–70% more effective than rotational energy, or translational energy, which is 2.5–3 times more effective than rotational energy in promoting adsorption. The measured internal state distributions for the rovibrational states listed above are consistent with the observed dependence of the kinetic energy of the desorbed molecules with the rotational state. In addition, the analysis performed yields the dependence of the adsorption probability on kinetic energy separately for each rovibrational state. These functions have very similar sigmoidal shapes for all states examined. Changing the quantum state is primarily associated with a shift in the position, or threshold energy, for the curves. The level at which these functions saturate or level off at high energy is independent of rotational state but varies nonmonotonically with the vibrational state.

I. INTRODUCTION

Numerous studies, theoretical and experimental, have been performed to understand energetic requirements and energy disposal in elementary chemical reactions. Although the majority of this work has been concerned with gas-phase systems,[1,2] recent developments in theoretical and experimental techniques have also allowed the dynamics of gas–surface reactions to be examined.[3,4] Over the past century and a half the chemisorption of H_2 on copper has become a model for the investigation of gas–surface dynamics, particularly for the development of a dynamical description of activated adsorption.[5–7] An important characteristic of the hydrogen/copper system is its relatively large barrier to adsorption. The theoretical estimate of ~ 1 eV for the barrier height[8] is consistent with direct adsorption measurements[9–12] and with desorption measurements that demonstrate highly peaked angular distributions[13–16] and high mean kinetic energies of desorbed molecules.[15] Recent work has focused on understanding how translational and vibrational energy promote H_2 (and D_2) adsorption on copper.[9–12,17–26] More specifically, these studies have led to a firm understanding of the effect of increasing vibrational energy on the translational energy threshold to adsorption. These results have been found to agree qualitatively, via detailed balance, with trends in experimental values[27] of vibrational population ratios of desorbed molecules.[17,20] Such information can be used as a basis for establishing the topography of the potential energy surface of this system.[24,25] This paper focuses on the role of rotation with respect to that of vibration and translation in dissociative adsorption and associative desorption. In particular, we present the results of experiments designed to determine the influence of rotational energy relative to the effect of vibrational and translational energy on the probability of adsorption.

The role of rotation in chemical reactions is an area of molecular reaction dynamics that has been extensively investigated theoretically. Numerous calculations have been performed using quantal, classical, and quasiclassical trajectory calculations.[1,28] In contrast, experimental investigations of rotational effects have been scarce. Of the experiments that have been performed to study these effects, nearly all have been concerned with the dynamics of bimo-

[a]Also affiliated with Department of Chemistry, Stanford University, Stanford, CA 94305.

 0021-9606/93/108294-14$06.00

lecular gas-phase reactions. The majority of these experiments have been carried out to determine the disposal of rotational energy into products.[28–35] Because of the practical difficulty of preparing reagent molecules in specific rotational states, relatively few experimental studies have investigated how reagent rotational motion can promote or inhibit a chemical reaction. Despite the paucity of experimental data, trends related to reagent rotation have been observed.[28] For most direct bimolecular reactions rotation appears to decrease reactivity at low rotational states, J, but increases it for high J states.[36–41] That is, the reaction rate or reaction cross section decreases from $J=0$ with increasing J and then increases after reaching a minimum. For systems, such as $Na+HF \rightarrow NaF+H$, that do not have a large anisotropic well in the entrance channel, this minimum often occurs near $J=4$ to 7 for HF. Theoretical studies have supported these observations.[42–60]

Gaining a complete understanding of these effects, however, is impossible without experimental data relating the influence of vibrational, translational, *and* rotational energy on the reaction probability. No experimental study has assessed the relative importance of all reagent degrees of freedom for chemical reactivity under the same experimental conditions. Though several experiments have addressed the issue of the effect of vibrational and rotational energy on reaction probability, none have been performed at more than a few selected collision energies, which limits conclusions that can be drawn about the influence of translational energy on the energetic requirements for reaction.

Experimental work directed at identifying the effect of molecular rotation on gas–surface reactions has been even less common than for gas-phase reactions. Many measurements have been made of the probability of dissociative adsorption as a function of incidence kinetic energy.[3,9–12,61] A few of these experiments have yielded additional information about the influence of vibrational energy on this process.[9,11,12,62–67] Experimental information about the role of rotation in surface reactions, on the other hand, has come predominantly from measurements of rotational distributions of desorbed molecules.[27,68–73] Typically these distributions are found to be slightly "colder" than the surface temperature. That is, the measured distributions display higher populations in the low rotational states than expected for a Boltzmann distribution at the surface temperature. Via the principle of detailed balance these results suggest that adsorption is generally slightly favored for low rotational states over high rotational states. Such measurements, however, cannot provide unambiguous information about the influence of translational energy on adsorption, which is essential to understanding the dynamics of the adsorption process.

We have obtained specific information about the role of translational energy in adsorption by recording time-of-flight (TOF) distributions of desorbed molecules and using the principle of detailed balance to analyze these data. Since we recorded these TOF distributions state selectively, we have been able to determine the effective translational barrier to adsorption for each rovibrational state, thus establishing the relative efficacy of translational, vibrational, and rotational energy for adsorption. Similar measurements have been performed previously by Schröter *et al.*[68,74] for H_2, HD, and D_2 desorbed from Pd(100), a system that does not possess a significant activation barrier to adsorption. As expected for a system with no activation barrier, the difference between the mean energy of the molecules desorbed from the surface and a thermal distribution at the surface temperature is small for all internal states measured. These results demonstrate that the effective translational barrier to adsorption is independent of the rotational state for the H_2/Pd(100) system.

In this paper we present results of similar experiments performed on the H_2/Cu system, which, in contrast to the H_2/Pd system, has a significant activation barrier to adsorption.[8] Preliminary results of these experiments were reported previously.[18] We report here TOF and internal state distributions of $D_2(v,J)$ desorbed from Cu(111) for rotational states $J=0$–14 for $v=0$, $J=0$–12 for $v=1$, and $J=0$–8 for $v=2$. In contrast to the results for H_2/Pd(100), the mean kinetic energy of D_2 desorbed from Cu(111) depends strongly on both vibrational and rotational states. Analyzing these results in terms of adsorption probabilities confirms the previous observations that vibrational energy is effective, though less effective than translational energy, in assisting molecules in surmounting the barrier to adsorption.[12,17] In addition, this analysis yields the interesting new result that the translational threshold to adsorption increases as J is increased from 0 to ~ 5 and then decreases with increasing J. Thus, rotation hinders adsorption for low rotational states ($J<5$) and enhances adsorption for high rotational states ($J>5$). This trend is the same as that observed for direct bimolecular reactions, as described above.

II. EXPERIMENTAL PROCEDURES AND DATA ANALYSIS

Experiments were performed in a UHV apparatus configured to allow the determination of quantum state and kinetic energy distributions of molecules desorbed from a single-crystal surface. D atoms were supplied to the surface via permeation through the bulk of the crystal. The flux of D_2 molecules leaving the surface was probed by laser ionization detection in a differentially pumped chamber. Energy distributions were determined from TOF distributions, which were measured by recording the flight times of photoions from their point of formation in a field-free region to a multichannel plate detector. Quantum state distributions were determined by comparing relative signal intensities for each quantum state desorbed from the surface with the corresponding signals obtained with an effusive (Knudsen) source of molecules that could be positioned in the same place as that of the crystal. A schematic drawing of the apparatus with the copper crystal in the position for recording TOF distributions is shown in Fig. 1.

A. Permeation source

The permeation source and heater assembly employed in this study was the same as that used by Kubiak, Sitz, and Zare.[27] It consisted of a 1 cm diameter Cu single crys-

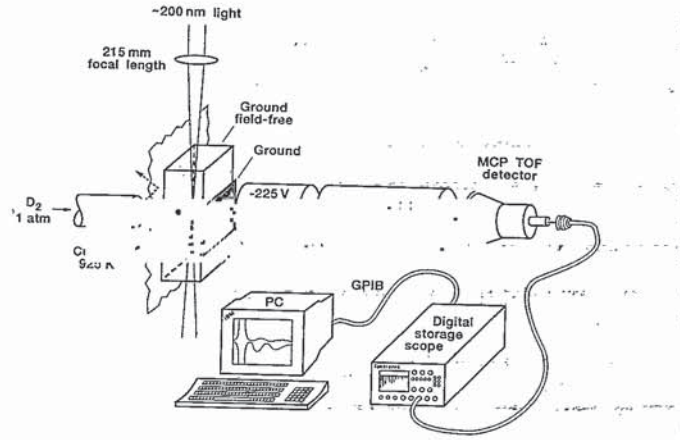

FIG. 1. Schematic drawing of the experimental apparatus.

tal electron beam welded to one end of a copper cylinder. The other end of the cylinder was brazed to a stainless steel tube, which in turn was connected to the D_2 gas supply. The source assembly was held on a manipulator that allowed the sample to be accurately positioned in front of the detection region or moved to the Auger/sputter region. The crystal surface was reoriented and repolished for the present study. After this procedure, the final orientation of the crystal was within 0.2° of the nominal (111) plane[75] and was ~0.8 mm thick.

The crystal surface was cleaned by Ar^+ ion bombardment, and contamination levels were determined using Auger electron spectroscopy (AES). Immediately after sputtering, surface impurities (carbon, sulfur, chlorine, etc.) were usually below the ~0.01 monolayer (ML) limit of detection of our AES system, where 1 ML~1.5×10^{15} cm^{-2}. After performing desorption experiments for many hours, low levels of contamination were sometimes evident, which corresponded to contamination levels of up to 0.05 ML. In most cases, however, contamination levels remained below the limit of detection of AES. The crystal was also examined via low energy electron diffraction (LEED) at the outset of this study; a sharp 1×1 pattern characteristic of a clean, well-ordered surface was observed.

The permeation source was heated radiatively by a coil of tantalum wire held in a spiral channel machined in a boron nitride cylinder.[76] The sample temperature was determined using two Chromel–Alumel thermocouples attached to the body of the source, which agreed to within approximately 2 K. For all experiments reported here the surface temperature was held close to 925 ± 5 K. At such temperatures, 1 atm of D_2 behind the sample gave an estimated flux of about 10^{15} molecules/s from the crystal. From variations in signal levels in the differentially pumped chamber associated with moving the crystal, we concluded that this flux comes from essentially the entire crystal face instead of a small region near the crystal center. The flux from the sides of the copper cylinder was ~1/4 of the flux from the crystal. When the permeation source was heated to 925 K, the pressure in the main chamber rose from a base pressure of 9×10^{-11} to 3×10^{-8} torr.

B. Laser and optics

D_2 molecules were detected in a quantum-state-specific manner by laser ionization via a two-photon resonance to the D_2 $E,F\ ^1\Sigma_g^+$ state.[77] All measurements were made using $(0,v)$ bands, where v is the vibrational state of the ground electronic state of the species under study. This scheme required light with a wavelength between 200.9 nm [for $Q(0)$ of the (0,0) band] and 215.3 nm [for $Q(8)$ of the (0,2) band]. This light was obtained from a Nd:YAG-pumped dye laser (Quanta-Ray, DCR2/PDL1) (where YAG denotes yttrium aluminum garnet), which was frequency tripled using a combination of KDP and BBO nonlinear crystals. We typically obtained about 1.7 mJ/pulse with a bandwidth ~0.5 cm^{-1} [full width at half maximum (FWHM)] a pulse duration of 8 ns, and a repetition rate of 10 Hz. Dye solutions were made from mixtures of R610 and SR640 (Exciton) dissolved in methanol (201 to 204 nm), R640 and DCM (Exciton) in methanol (203 to 208 nm), and pure DCM in methanol (>208 nm).

The laser beam was directed approximately 4 m to the apparatus using four mirrors (Acton Research Corp.), each of which reflected about 95% of the radiation between 201 and 215 nm and transmitted more than 90% of residual visible and near UV light. The resulting beam was reduced in diameter slightly with a circular aperture before it reached the focusing lens at which point it had a power of about 1.2 mJ/pulse in a ~1 cm diameter spot. Almost all visible or near UV radiation was discarded before reaching the focusing lens. The detection beam was focused with a single plano-convex suprasil lens with a nominal focal length of 250 mm. In the wavelength range of 200–215 nm the measured focal point was 215 mm from the lens. The beam passed through the chamber via two UHV suprasil windows (Insulator Seals), which were found to transmit more than 90% of this radiation when clean. To maintain cleanliness, both windows were routinely heated to about 370 K between experiments.

C. Ion collection and data acquisition

A key aspect of our study was the determination of the time-of-flight (TOF) distributions of the desorbed molecules. These measurements were made by recording the flight times of the photoions under conditions where the overall flight times were dominated by the flight times of the ions in a nominally field-free region. This region was separated from the sample chamber by a wall that allowed desorbed molecules to enter only through a 6 mm aperture placed 7 mm from the surface. A plate made from 0.25 mm tantalum covered the wall in the region of this aperture. The region was about 80 mm high, 28 mm wide, and 28 mm long. This structure was open at both ends to allow the laser to pass. See Fig. 2. The three remaining sides of the field-free region were formed from gold-plated tungsten mesh (0.025 mm wire, ~1.4 strands/mm, >90% transmission) held on a frame made from 2 mm strips of 0.25

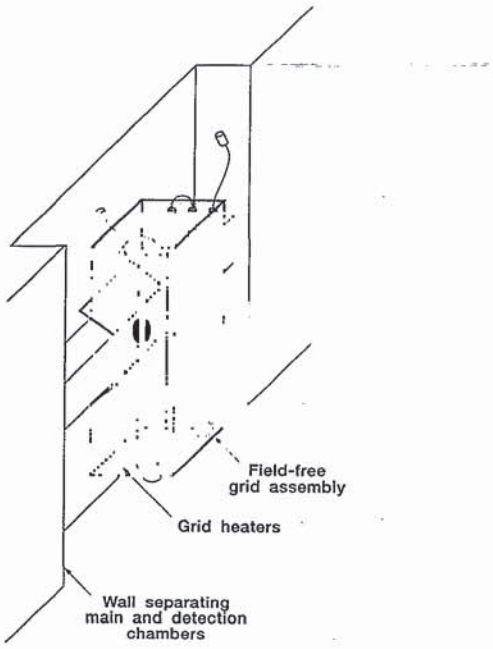

FIG. 2. Pictorial drawing of the field-free grid assembly.

mm thick tantalum foil. The whole assembly, including the aperture plate, was coated with colloidal graphite applied as an alkaline aqueous suspension in an ultrasonic bath. In addition, all components could be heated, using 0.25 mm tantalum wire insulated by ceramic tubes. In order to obtain relatively undistorted and reproducible TOF distributions (or thermal distributions from the Knudsen source), it was necessary to keep these components free of adsorbed contaminants that could create patch fields. The ion optics were thus heated at all times. The back plate was heated with about 10 W, and the mesh structure was heated with about 3 W applied to each of the two sides adjacent to the wall. We believe that this power was sufficient to keep all parts at a temperature greater than 400 K.

The laser passed through this region about 6 mm from the aperture plate and about 22 mm from the grid opposite the aperture. Suitably directed photoions continued field-free flight to a single grounded grid placed 2 mm further from the laser (see Fig. 1). Those ions passing through this grid were then accelerated to a simple electrostatic lens formed from two sections of a 7.5 cm diameter tube aligned along the line defined by the crystal surface, aperture, and laser ionization zone. The first tube was 8 cm long, and its end closest to the grounded grid was covered with the same mesh, which was thus parallel to the single grounded grid and 1 cm from it. This tube was held at a ground potential until 700 ns after the laser pulse, at which point it was raised to a potential of -225 V with a ~ 200 ns rise time. This delay in supplying a voltage to the first stage of the collection optics did not affect the collection of D_2 photoions because the delay was shorter than the time spent by the photoions in the field-free region. The delay did, however, prevent collection of heavier ions created by photodesorption by scattered light of contaminant molecules adsorbed on the walls of the ion optics. Without the voltage delay, these ions, though heavier, would arrive at the detector at about the same time as the D_2 signal because of their shorter flight path. The second tube was 15 cm long and positioned 3 cm from the end of the first tube. Ions entering the first tube were focused through a 1 cm hole in a tantalum sheet placed over the far end of the second tube by maintaining a voltage of about -1670 V on the second tube. Ions passing through this hole were then accelerated onto a multichannel plate (MCP) detector (Gallileo Electro-Optics Corp., FTD2003) whose cathode was held at a slightly higher negative potential (-1700 V) to prevent photoelectrons liberated in the tube assembly from being drawn onto it. Figure 1 displays a schematic drawing of the ion collection geometry.

Signals from the MCP detector were amplified by a factor of 25 with a fast preamplifier (Stanford Research Systems, Inc., SR440) and then fed to a digital storage oscilloscope (Tektronix, 2440). This instrument was operated in the "envelope mode" in which it records the maximum signal per channel. On the time range that was used, 2 μs/cm, the time resolution is 80 ns/channel. The signal sensitivity was typically set to 20 mV/cm. Every laser shot generated a TOF distribution, which was transferred to a personal computer (IBM, PS/2). These data were averaged in real time until adequate signal-to-noise (S/N) levels were reached. For large signal, e.g., for $J=4$ of $v=0$, the average of 2500 laser shots gave curves with a S/N ratio of approximately 100:1. For the lowest signals recorded, e.g., for $J=8$ of $v=2$, 25 000 shots (requiring almost 1 h) gave a S/N ratio of approximately 10:1. Data were uploaded to a mainframe computer (IBM 3090-600) for analysis.

D. Time-of-flight analysis

The method of equating ion TOF distributions with those of their neutral counterparts has been used successfully in several previous studies and is a valuable tool in gas–surface dynamics. It appears to have been first employed by Häger, Shen, and Walther[78] to measure the velocities of NO molecules scattered from graphite. More recently, Schröter *et al.*[68,74] have applied the method to measure the TOF distributions of H_2 and D_2 desorbed from a Pd(100) surface. Although potentially reliable, this method requires considerable care to avoid undue perturbation of the ion velocities by stray fields. The ion TOF distributions obtained in our initial experiments clearly displayed distortions, particularly for energies below approximately 50 meV. With the ion collection assembly described above, however, such distortions were found to be relatively small and confined to energies below approximately 35 meV. Since D_2 molecules desorbed from Cu(111) generally had much greater energies, the remaining distortions were essentially negligible. The most significant problem appeared to be one whereby ions were deflected by small electric fields perpendicular to their flight direction and were thus prevented from hitting the detector. Low energy ions are deflected more easily than high energy ions, and thus the TOF distributions measured from the effusive source were found to be slightly distorted

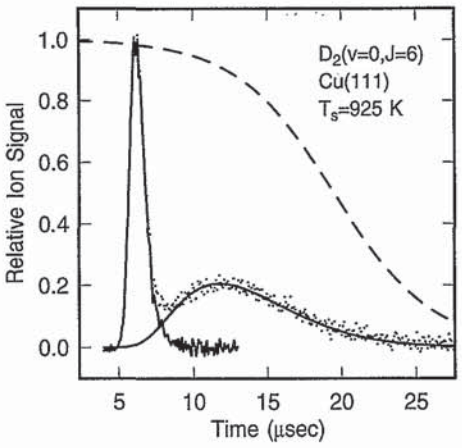

FIG. 3. Time-of-flight distribution of $D_2(v=0, J=6)$ desorbed from Cu(111). This TOF distribution recorded for $D_2(v=0, J=6)$ shows a second peak resulting from ionization of ambient D_2. The solid curve shows a Maxwellian velocity distribution expressed as a function of time and modified by the "cutoff" function, which is fit to the second peak and then subtracted from the measured TOF distribution during the initial stages of the data analysis. The dashed curve represents the cutoff function described in the text with $t_c=19.5$ μs and $t_w=6.6$ μs.

by loss of low energy ions. Such a distortion of a thermal distribution can be computationally reproduced by multiplying the Maxwellian velocity distribution (expressed as a function of time) by a "cutoff" function that attenuates signals associated with flight times longer than a time t_c. The function $1-\tanh[(t_i-t_c)/t_w]$ is adequate for this purpose, where t_i is the ion flight time, and t_w is a "width" parameter, which smooths the attenuation. An example of this function is represented by the dashed line in Fig. 3. In practice, t_c was always much longer than the times at which signals are observed for D_2 desorbed from Cu(111) and thus did not have a significant effect on the shape of the desorption peak.

To obtain distributions we believe to be characteristic of desorbed D_2, we first subtracted from each TOF wave form a distribution obtained with the laser tuned off the D_2 line. This procedure removes a relatively small contribution at long times associated with the nonresonant ionization of other gases present in the system. In addition, this subtraction removes most of the photoelectron peak at early times that is caused by scattered 200 nm light reaching the MCP cathode. For most (v,J) levels this procedure was sufficient. For states that had substantial populations in the ambient D_2 gas, we observed a distinct second peak in the TOF distribution. An example is shown in Fig. 3. This peak was fit by a Maxwellian velocity distribution (expressed as a function of time and modified by the cutoff function). The fitted curve was subtracted from the recorded TOF distribution to give a single well-defined TOF peak.

Such peaks were analyzed in a number of ways. Considering the results in the context of desorption, we fit the observed TOF distributions by a velocity distribution function corresponding to a shifted Maxwellian velocity distribution converted from velocity to time. Here the flux at velocity V is given by

$$F(V)dV=K_V V^3 \exp[-(V-V_s)^2/\alpha^2]dV, \quad (1)$$

where K_V is a proportionality constant, V_s is a stream velocity, and α is a width parameter. A nonlinear least-squares fitting algorithm returns V_s and α. The resulting fits agree very well with the data, indicating that Eq. (1) has adequate flexibility to describe the observed distributions.

E. Adsorption probability as a function of energy, S_0

In order to relate the observed TOF spectra to adsorption measurements, we analyzed the data in terms of an adsorption probability function, $S_0(E_i,\theta_i,v,J)$, using the principle of detailed balance.[17] Detailed balance, when applied to adsorption/desorption processes, states that for a system at equilibrium the rate of adsorption is equal to the rate of desorption for any subset of molecules of the equilibrium flux striking the surface.[79] It has been shown that the principle of detailed balance can be applied to relate adsorption/reflection measurements to desorption measurements made on systems at equilibrium[80–83] and quasi-equilibrium, e.g., under conditions established in a molecular beam experiment.[17,82,84–89] In this study we used detailed balance to extract information about adsorption dynamics from the TOF distributions of molecules desorbed from the surface.

According to detailed balance, the TOF distribution is given by the product of the flux-weighted velocity distribution related to the surface temperature and the adsorption probability function, $S_0(E_i,\theta_i,v,J)$, that associates the adsorption probability with the translational energy of molecules in a particular quantum state striking the surface. E_i and θ_i represent the incidence energy and angle, respectively. The signal detected at time t and polar angle θ_i relative to the surface normal in internal state (v,J) is given by[17]

$$f(t,\theta_i,v,J)dt=K_t\left(\frac{x}{t'}\right)^4 \exp\left(-\frac{E_i}{kT_s}\right)\cos\theta_i \times S_0(E_i,\theta_i,v,J)dt, \quad (2)$$

where K_t is a proportionality constant and $E_i=1/2m(x/t')^2$. Here x is the distance the molecule travels as an ion in the field-free region, T_s is the surface temperature, m is the mass of the molecule, $t'=t-t_{cor}$, and t_{cor} corrects to the true zero time by allowing for the ion flight time after the molecules leave the field-free region. Note that Eq. (2) applies when the detector is sensitive to density instead of flux, which would require an additional factor of (x/t'). We determined $S_0(E_i,\theta_i,v,J)$ by fitting the TOF distribution with Eq. (2) summing over our angular resolution, which we estimated to be approximately 20°.

We obtained quantitative information about the adsorption function by using a flexible analytical form for the adsorption vs energy function for each (v,J) state. We used

$$S_0(E_i,\theta_i,v,J)=\frac{A(v,J)}{2}\left\{1+\mathrm{erf}\left[\frac{E_n-E_0(v,J)}{W(v,J)}\right]\right\}, \quad (3)$$

where E_n is the "normal energy" given by $E_n=E_i\cos^2\theta_i$. E_0 is the kinetic energy required for the adsorption probability to reach half its maximum value, and W is a width parameter that controls the steepness of the function. The parameter $A(v,J)$ is a global scaling factor ($\leqslant 1$) that establishes the asymptotic value of $S_0(E_n,v,J)$ at high kinetic energy. This function is slightly different from that employed in our previous studies,[12,17,90] where a tanh function was used in place of the erf function. The error function reproduces the form of the adsorption function better at low energies than does the hyperbolic tangent function (which falls off more slowly at low energy), particularly for desorbed $D_2(v=0)$. The application of the model involved a separate calculation for each measured TOF point that included a convolution over the angular resolution of the apparatus. The parameters of the model, E_0 and W, were then adjusted by a nonlinear least-squares procedure to achieve the best agreement with the data.

F. Internal state distributions from S_0

We used $S_0(E_n,v,J)$, determined from the TOF distributions, to calculate relative populations of molecules desorbed into individual internal states. To do so, we multiplied $S_0(E_n,v,J)$ by the flux-weighted Maxwellian velocity distribution corresponding to the surface temperature and by the Boltzmann factor for internal state (v,J) at temperature T_s and then integrated over energy and angle. The relative density of desorbed molecules populating state (v,J) was thus calculated with[17]

$$P(v,J)\propto\int_0^{\infty}\int_0^{\theta_c}\sqrt{E_i}\exp\left(-\frac{E_i}{kT_s}\right)\exp\left[-\frac{E(v,J)}{kT_s}\right]$$
$$\times S(E_i,\theta_i,v,J)\cos\theta_i\sin\theta_i\,d\theta_i\,dE_i. \quad (4)$$

E_i is a kinetic energy as defined above, T_s is the surface temperature, $E(v,J)$ is the internal energy for state (v,J), θ_i is the polar angle, and θ_c is dictated by the geometrical constraints of the experiment ($\sim 20°$ for this experiment). These calculated distributions were then compared with measured distributions. Deviations between measured and calculated distributions were used to determine relative values of $A(v,J)$.

III. RESULTS

A. Rotational distributions

We measured rotational distributions for $D_2(v=0,1,$ and $2)$ desorbed from Cu(111) at $T_s=925$ K. These distributions are displayed in Fig. 4 in a plot of $\ln[N/g_n(2J+1)]$ vs the rotational energy, where N is the calibrated signal, and $g_n(2J+1)$ is the statistical weight for rotational level J ($g_n=2$ for even J and 1 for odd J). A Boltzmann distribution would follow a straight line on this plot. The measured distributions (open symbols) deviate substantially from the Boltzmann rotational distributions corresponding to the surface temperature (solid lines), particularly for $v=0$. These deviations demonstrate that there are significant rotational effects. Also shown in Fig. 4 are the measurements of Kubiak, Sitz, and Zare[27] (plus marks) for the same isotope and crystal face though slightly higher surface temperature (960 K). Although Kubiak, Sitz, and Zare lacked the detection sensitivity to measure rotational distributions for $v=0$ and 2 and higher rotational states of $v=1$, our data nearly coincide with their populations measured for $v=1$. The measured rotational distributions, particularly for $v=0$ and to a lesser extent for $v=1$, have higher population in the lowest rotational states ($J=0$–2) than expected for a thermal distribution at the surface temperature of 925 K. These distributions, in addition, have enhanced population in high rotational states ($J=9$–14). The deviation from the thermal distribution increases with decreasing J at low J and with increasing J at high J. The $v=2$ rotational distribution, however, does not deviate significantly from a Boltzmann distribution.

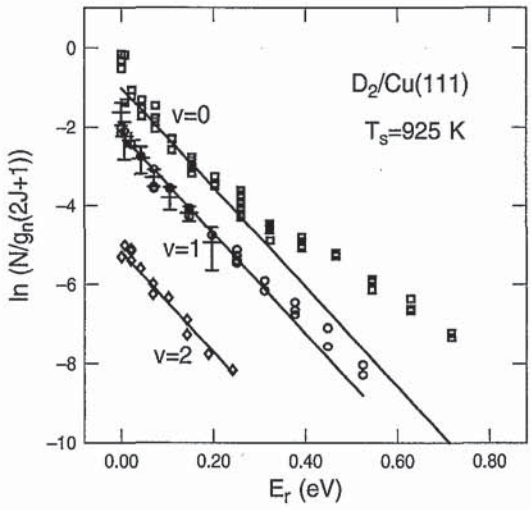

FIG. 4. Desorption rotational state distributions. Boltzmann plots of rotational distributions are shown for several vibrational states. The squares represent the distribution recorded for $v=0$, the circles for $v=1$, and the diamonds for $v=2$. The plus signs show the values recorded by Kubiak, Sitz, and Zare (Ref. 27) for $v=1$. The lines represent the rotational Boltzmann distributions at the surface temperature.

B. TOF distributions

As discussed in Sec. II E, the translational energy of desorbed molecules is related to the translational threshold to adsorption. Thus, by measuring the kinetic energy of molecules desorbed from the surface for each rovibrational state, we can determine the effective translational barrier, i.e., the amount of translational energy required for adsorption, for each state. Shown in Fig. 5 are TOF distributions of $D_2(v=0)$ desorbed from Cu(111) into different rotational states. Figure 6 displays distributions for the $J=2$ state of different vibrational states. As can be seen in Figs. 5 and 6, the TOF distributions change substantially with both vibrational and rotational state. In the case of Fig. 5, the dashed line drawn through the peak of each distribution emphasizes the shift of the distributions to ear-

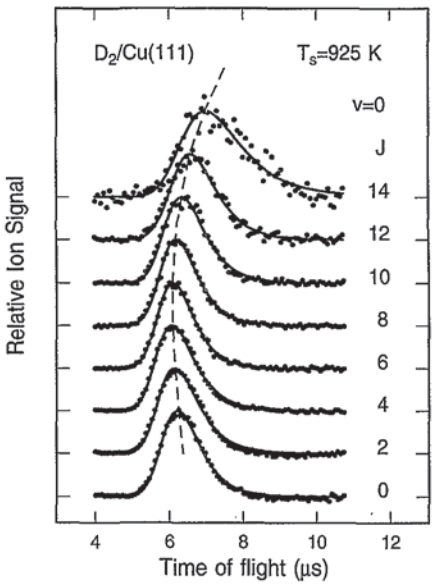

FIG. 5. Desorption TOF distributions of selected rotational states. This figure displays time-of-flight distributions obtained for D_2 desorbed from Cu(111) in different rotational states of the ground vibrational state. The solid lines show fitted distributions based on the adsorption function given in Eq. (3). The dashed line passes through the peak of each distribution as a guide to the eye.

lier time as J is increased from 0 to 6 and to later time as J is increased from 6 to 14. The shift of the distributions with v and J is summarized in a plot of the mean translational energy [determined from fitting Eq. (1) to each TOF distribution] against J in Fig. 7. This figure demonstrates that the mean translational energy depends strongly on both vibrational and rotational states. In the case of vibration, for $J=2$ the mean energy decreases from 0.595 for $v=0$ to 0.411 for $v=1$ and to 0.273 for $v=2$, with an absolute uncertainty of $\sim 10\%$ and a relative uncertainty

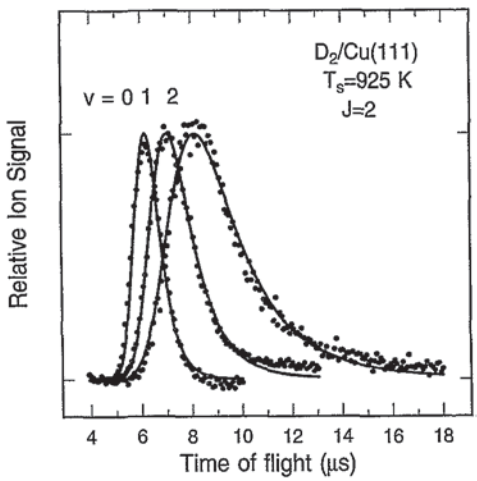

FIG. 6. Desorption TOF distributions of $J=2$ for $v=0$, 1, and 2. This figure displays time-of-flight distributions obtained for D_2 desorbed from Cu(111) in a single rotational state and different vibrational states. The lines show fitted distributions based on the adsorption function given in Eq. (3).

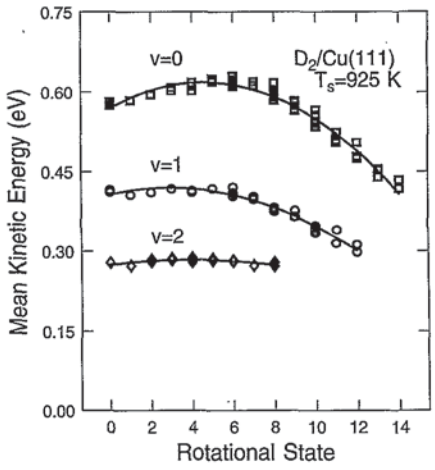

FIG. 7. Mean translational energy of $D_2(v,J)$ desorbed from Cu(111). The mean translational energy, obtained from fits of Eq. (1) to D_2 time-of-flight distributions for different rovibrational states, is plotted against rotational quantum number J.

of $\sim 1\%$. In the case of rotation, the mean energy is seen to increase with increasing J for $J<5$ and decrease with increasing J for $J>5$; this trend is most marked for $v=0$.

These results are consistent with the shape of the measured rotational distribution. We can describe the amount of translational energy required to make the transition from molecular reactants to adsorption products in terms of an effective translational barrier. By arguments based on detailed balance, the dependence of the mean energy on J implies that the effective translational barrier must increase with increasing J for low rotational states and decrease with increasing J for high rotational states. A lower effective barrier would lead to a higher probability of adsorption and hence to a higher population in desorption. Thus, if the barrier increases with increasing the rotational state for $J<5$, the populations should decrease with increasing the rotational state for $J<5$, as observed. Similarly, as the effective barrier decreases, the populations should increase with increasing the rotational state for $J>5$.

C. The variation of $S_0(E_n,v,J)$ with the rotational state

A more quantitative way of completing the analysis of the translational energy requirements for adsorption entails fitting the TOF distributions with Eq. (2) to extract $S_0(E_i,\theta_i,v,J)$, the dependence of the adsorption probability on translational energy for each rovibrational state. This analysis yields a quantitative estimate of the translational threshold, $E_0(v,J)$, and thus the effective translational barrier to adsorption. As expected, the values of $E_0(v,J)$ that are extracted in this analysis demonstrate the same behavior with J as do the values of the mean translational energy. They increase with increasing J at low J and decrease with increasing J at high J. Figure 8 shows $E_0(v,J)$ plotted as a function of J for each vibrational state. In contrast to the rotational distributions (Fig. 4) and the mean energies (Fig. 7), the J-dependent trends observed for $E_0(v,J)$ do not diminish substantially with increasing v. The width

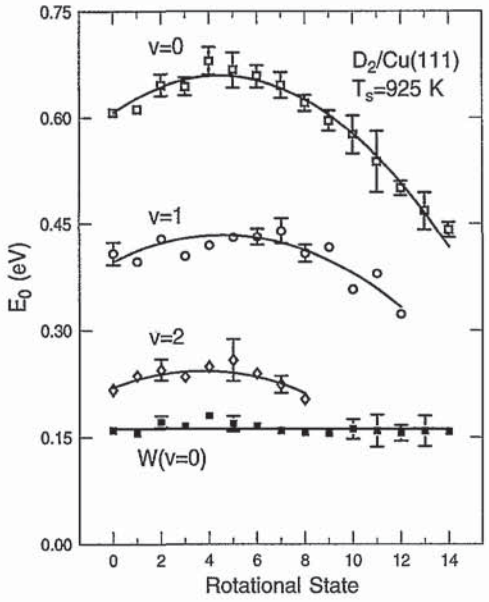

FIG. 8. Dependence of the translational threshold on v and J. Values of the translational threshold, E_0, obtained from fits of Eq. (2) [using Eq. (3) for S_0] to D_2 time-of-flight distributions for different rovibrational states, are plotted against rotational quantum number J for vibrational states $v=0$, 1, and 2. The lines represent quadratic fits to the points performed for each vibrational state. Also shown are the values of $W(0)$, the functional width of Eq. (3) for $v=0$, derived from the fits of Eq. (2).

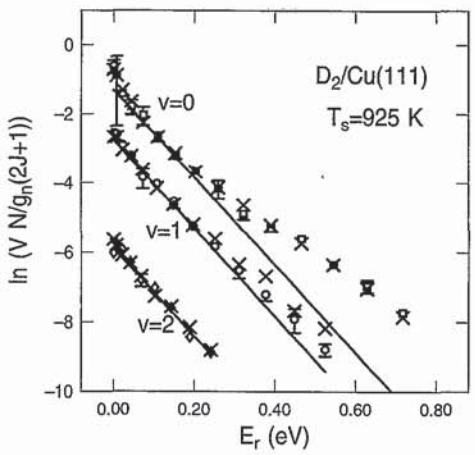

FIG. 10. Desorption rotational state distributions corrected for velocity. Boltzmann plots of rotational distributions corrected to correspond to flux instead of density are shown for several vibrational states. The lines represent the rotational Boltzmann distributions at the surface temperature: open symbols, the measured distributions; ×'s, the distributions calculated using detailed balance and $S_0(E_n,v,J)$ derived from the time-of-flight distributions.

parameter, on the other hand, is nearly independent of J. Values of $W(0)$, the functional width for $v=0$, are plotted against J in Fig. 8, as an example to demonstrate that this parameter does not vary significantly with J. The same type of behavior is seen for $W(1)$ and $W(2)$ but is not shown in this figure.

The dependence of the adsorption probability on translational energy is presented graphically in Fig. 9, where $S_0(E_n,v=0,J)$ is plotted against E_n for several representative rotational states. Curves with larger translational thresholds will be shifted to higher E_n in this figure. Since the widths do not depend significantly on rotational state, the shapes of these curves are similar. Here, the curves have been plotted with the same global normalization, i.e., the value of $A(v,J)$ from Eq. (2) has been assumed to be independent of rotational state. Although the values of $E_0(v,J)$ and $W(v,J)$ are determined by the shapes of the TOF distributions, the relative values of $A(v,J)$ depend on the relative intensities among the curves. Our measurements indicate that the values of A are independent of rotational state. This result can most clearly be demonstrated by comparing measured populations with rotational distributions calculated using Eq. (4) and a value of A that is independent of J. If A actually depended on J, then the rotational distribution calculated using a J-independent parameter A would not agree with the measured distribution. As can be seen in Fig. 10, the calculated distributions, represented as ×'s, agree closely with the experimental values, represented by the open symbols.

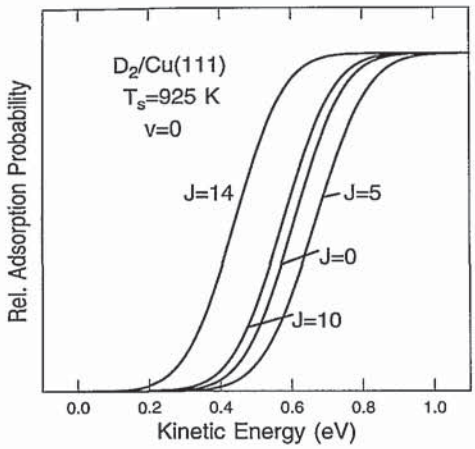

FIG. 9. Kinetic energy dependence of the adsorption probability. The internal-state-dependent adsorption probability function for D_2 on Cu(111), $S_0(E_n,v,J)$, is plotted against E_n for selected rotational states of the ground vibrational state.

D. The variation of $S_0(E_n,v,J)$ with vibrational state

As with the analysis presented above, Eq. (2) was fit to the TOF distributions for different vibrational states, such as those in Fig. 6, to yield $S_0(E_n,v,J)$ functions. Figure 11 displays $S_0(E_n,v,J)$ for $v=0$, 1, and 2 all with $J=2$. Placing vibrational energy in the incident molecule decreases the amount of translational energy required for it to adsorb. That the translational threshold depends strongly on vibrational state confirms conclusions that have been drawn previously from direct adsorption measurements[9,11,12,17,67] and trajectory calculations.[20–26] A comparison of the results of these desorption measurements with previous adsorption measurements is given in Sec. III F.

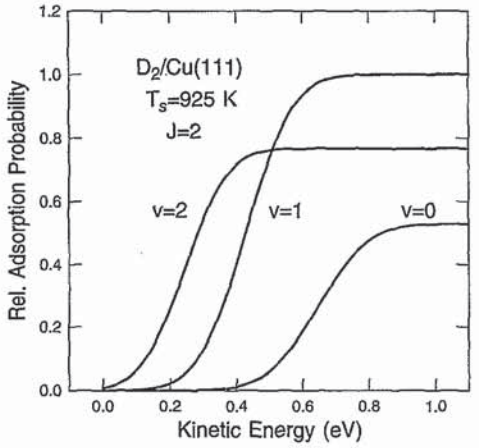

FIG. 11. Kinetic energy dependence of the adsorption probability. The internal-state-dependent adsorption probability function for D_2 on Cu(111), $S_0(E_n,v,J)$, is plotted against E_n for a single rotational state ($J=2$) and several vibrational states ($v=0$, 1, and 2).

E. Vibrational distributions

As can be seen in Fig. 11, the saturation level, the value of the adsorption probability at which each adsorption function asymptotically approaches a maximum, is defined by the parameter A and varies with vibrational state. Although the desorption measurements do not give absolute values of $A(v)$, the relative intensities of the signals for different internal states do yield relative $A(v)$ values. We derived $A(v)$ by comparing measured vibrational population ratios with those predicted using Eq. (4) and $S_0(E_n,v,J)$ determined from fitting Eq. (2) to the TOF distributions. Summing the measured populations of the first nine rotational states of each vibrational state gives a vibrational population ratio of 0.015 ± 0.004 for $D_2(v=2)/D_2(v=0)$ and 0.25 ± 0.07 for $D_2(v=1)/D_2(v=0)$, which is within the uncertainty of the value obtained by Kubiak, Sitz, and Zare[27] of 0.35 ± 0.20. Using a value of A that is the same for all vibrational states yields predicted values of 0.0103 for $D_2(v=2)/D_2(v=0)$ and 0.135 for $D_2(v=1)/D_2(v=0)$. It is unlikely that experimental uncertainties are responsible for the discrepancies between the measured and predicted values. For the $D_2(v=1)/D_2(v=0)$ ratio assuming a surface temperature as high as 1000 K changed the predicted value by at most 15%. Likewise, taking the angular resolution to be 70° instead of the estimated 20° changed the predicted value by only 17%, in contrast to the 85% change necessary to achieve agreement with the measured value. Assuming that detailed balance works for this system, the only explanation for this discrepancy is that the value of A is different for different vibrational states. The ratios of the measured and predicted population ratios give relative $A(v)$ values, $A(0):A(1):A(2)$, of $(0.54\pm0.16):1.00:(0.77\pm0.18)$. The $\times$'s shown in Fig. 10 were calculated using these relative $A(v)$ values.

To make meaningful comparisons of internal state populations with corresponding Boltzmann populations, we need to account for the fact that our detection sensitivity is higher for species with lower velocities i.e., our detector is sensitive to density instead of flux. We have approximately corrected the distributions presented in Fig. 10 by multiplying each measured population by $(E_{ave})^{1/2}$. This correction makes little difference to the rotational distribution (as seen by comparing Fig. 10 with Fig. 4, which does not include the correction) but significantly influences the vibrational population ratios. Summing over $J=0$ to 8 for each vibrational state gives ratios of 0.20 ± 0.03 for $D_2(v=1)/D_2(v=0)$ and 0.0096 ± 0.0018 for $D_2(v=2)/D_2(v=0)$. The corresponding Boltzmann ratios are 0.0101 for $D_2(v=1)/D_2(v=0)$ and 0.000 122 for $D_2(v=2)/D_2(v=0)$, making vibrational enhancement a factor of 20 for $v=1$ and 79 for $v=2$ over the Boltzmann populations associated with a surface temperature of 925 K.

F. Comparison of $S_0(E_e,v,J)$ with adsorption measurements

The curves shown in Fig. 11 are very similar to those derived for this system from direct adsorption experiments in which adsorption probabilities were measured as a function of nozzle temperature and mean kinetic energy of the incident molecular beam.[12] In these experiments the translational energy was controlled independently from the vibrational energy by varying the nozzle temperature to change the Boltzmann populations and seeding in H_2 or heavier molecules to change the mean kinetic energy. It is very difficult, however, to generate a beam of D_2 that has high enough mean kinetic energy for molecules populating $v=0$ to access the barrier to adsorption. Thus, our ability to determine the translational threshold for $v=0$ using this method is limited. The present experiment, on the other hand, suffers less from this limitation; as long as the overlap of the thermal distribution at 925 K with $S_0(E_n,v=0)$ is large enough, we can establish $E_0(v=0)$.

Another advantage in deriving $S_0(E_n)$ from desorption TOF distributions is that each TOF distribution results from a single rovibrational state. In contrast, each direct adsorption probability measurement results from the adsorption of a number of internal states, making the determination of E_0, W, and A for each state complex. An analysis of direct adsorption measurements, such as that performed by Rettner, Auerbach, and Michelsen,[12] would be impossible if every rotational state contributing to the adsorption probability were considered separately. Because of the complexity of this type of analysis, Rettner, Auerbach, and Michelsen were forced to ignore the contribution from different rotational states and to assume that the parameter A was independent of the vibrational state. As discussed in Sec. III E, this parameter is not independent of the vibrational state. Nevertheless, the values of $E_0(v)$ derived from this analysis, 0.72 ± 0.10 eV for $v=0$, 0.41 ± 0.10 eV for $v=1$, and 0.23 ± 0.05 eV for $v=2$, are in the range of E_0 values established from the present experiment for the lower, more populated rotational states.

As a further check on the agreement between the results of this desorption study and the previous adsorption measurements, we have fit the direct adsorption measure-

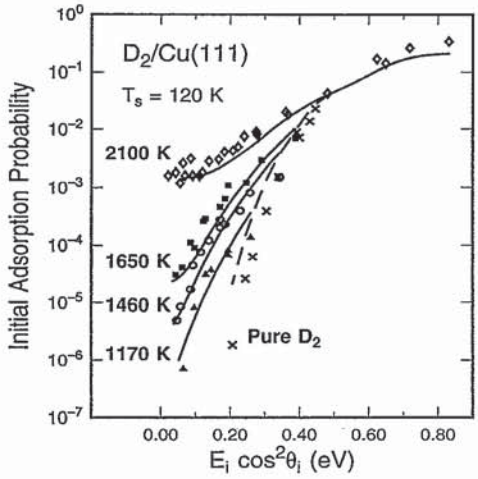

FIG. 12. Comparison of results from TOF analysis with direct adsorption results. The adsorption probability (in the zero coverage limit) for D_2 on Cu(111) is plotted against "normal energy," E_n. Data are shown for seeded beams recorded at incidence angles ranging from 0° to 60° and with four nozzle temperatures: 1170 K, solid triangles; 1460 K, circles; 1650 K, solid squares; 2100 K, open diamonds. The ×'s followed by the dashed curve represent data for pure D_2 expanded from a nozzle at temperatures ranging from 875 to 2100 K. The lines show the results of fits of $S_0(E_n,v,J)$ to these data in which only $W(v)$ and the global magnitude of $A(v)$ were allowed to vary. $E_0(v,J)$ and the relative values of $A(v)$ were constrained to the values derived from the desorption TOF distributions.

ments using $S_0(E_n,v,J)$ derived from the TOF desorption measurements. In this fit we allowed only $W(v)$ and the global (not relative) values of $A(v)$ to vary. The desorption measurements cannot give absolute values of $A(v)$ but can provide relative values of this parameter for the states measured. The ratio $A(0):A(1):A(2)$ was thus fixed at the value given in Sec. III E, but the absolute magnitudes of the values of $A(v)$ were allowed to vary. $W(v)$ was allowed to vary to account for surface temperature effects, which have been demonstrated to cause the width to increase with increasing surface temperature.[90] The agreement between the fit and the adsorption measurements, presented in Fig. 12, is good. The widths given by this fit to adsorption data recorded at a surface temperature of 120 K [$W(0)=0.117$ eV, $W(1)=0.119$ eV, $W(2)=0.102$ eV] are smaller than those obtained from the present study performed at 925 K [$W(0)=0.162\pm0.007$, $W(1)=0.164\pm0.016$, $W(2)=0.144\pm0.018$] by an amount that is consistent with surface-temperature trends observed previously.[90]

IV. DISCUSSION

For a system possessing a large activation barrier, such as the H_2/Cu system, adsorption would be expected to be sensitive to the internal state and kinetic energy of a molecule to overcome the barrier. Experimental and theoretical[20–26,91] studies have shown that both vibrational and translational energy promote adsorption. The results presented in the preceding section demonstrate that rotational motion also plays a significant role in the adsorption process. The relative efficacies of vibrational and translational energy can be explained by coupling between these degrees of freedom, which depends on the topography of the potential energy surface (PES). The effectiveness of rotational energy, on the other hand, is expected to be related to the anisotropy of the PES. Theoretical calculations have suggested that the H_2/Cu PES is highly anisotropic and that reaction occurs more readily when the molecular axis is parallel to the surface.[24,92,93] This conclusion is in agreement with that drawn from calculations of hydrogen interactions with a jellium surface.[94] How this anisotropy may lead to coupling of rotational motion to the reaction coordinate is discussed in Sec. IV A.

A. The effect of rotation on adsorption

The conclusion that rotation plays a role in the adsorption and desorption dynamics can be drawn solely by considering the rotational distributions shown in Fig. 10. The measured distributions deviate markedly from the rotational Boltzmann distributions at the surface temperature, represented by solid lines, particularly for $v=0$ (open squares) and to a lesser extent for $v=1$ (open circles). These measurements demonstrate a strong rotational dependence that can be attributed to the effect of the rotational state on the desorption and thus adsorption dynamics. The $v=0$ and $v=1$ measured rotational distributions show a larger enhancement in population over the Boltzmann distribution with decreasing J for $J<5$ and with increasing J for $J>5$. Invoking detailed balance, it could be argued that these trends are similar to those observed for gas-phase bimolecular reactions. That is, the probability of reaction decreases with increasing J for low rotational states and increases with increasing J for high rotational states. This conclusion is supported by the J-dependent behavior of the mean energy of the desorbed molecules but is most clearly emphasized by the change in $E_0(v,J)$ with J. These results show that the amount of translational energy needed to surmount the adsorption barrier increases with increasing J at low J and decreases with increasing J at high J. These trends do not change substantially with vibrational state.

Trajectory calculations for gas-phase reactions have shown that reagent molecules in low rotational states are highly sensitive to the anisotropy of the potential,[42–60] indicating that the effect observed at low J is a steric or "orientational" one. This effect can be explained simply by considering the amount of time the reactants can remain in a preferred configuration (sometimes called the cone of acceptance) during the reactive collision. If the potential is anisotropic and the cone of acceptance small under the collision conditions investigated, the reacting pair must encounter one another in a specific geometry to react. Rotational motion then restricts the reactants' ability to maintain a specific approach geometry during the critical collision time and inhibits the reaction.[38,95–97] At higher J the amount of time spent in a favorable orientation will be independent of J (a rotating reagent diatomic molecule will become a "blur" to its reactant partner), and the stereodynamic effect is expected to be less important than the "energy" effect. The energy effect, which we believe to be responsible for enhanced reactivity at high J, depends on a

coupling of rotational motion to the reaction coordinate. Thus, a transfer of rotational to translational energy during the reactive collision will enhance the reaction probability for a system with an early barrier by effectively increasing the collision energy. Similarly, an increase in reactivity with increasing J would be expected if rotation were coupled to vibration for a system with a late barrier. Either coupling could apply to the H_2/Cu system.

Similarly to the gas-phase case discussed above, rotational motion for low J states may hinder adsorption by restricting the amount of time the molecule spends in a favorable orientation relative to the surface. Estimates of the angle over which a molecule rotates during a reactive encounter can be made by assuming an incidence velocity and distance along the PES over which the molecule reacts. For example, a $D_2(J=6)$ molecule with an incidence energy of 0.6 eV will rotate through $\sim 40°$ over an estimated reactive distance of ~ 0.5 Å, while a $D_2(J=1)$ molecule with the same incidence energy will only rotate $\sim 9°$ during the reactive collision. In addition, since the translational energy is lower for molecules adsorbing from higher vibrational states, these molecules will spend more time in the reactive region of the potential and thus will undergo more rotation during the adsorption process. The limit at which the molecule becomes a "blur" should therefore shift to lower J with increasing v (by about one J with each v). The result would be a small effect, which in this case would be overwhelmed by the profound high J trend.

There are two ways in which a stereodynamic effect could reduce the adsorption probability: either (1) a narrow cone of acceptance restricts the number of trajectories that adsorb or (2) molecules can adsorb if they approach the surface with unfavorable molecular orientations, but they require more translational energy to do so. The former case would likely cause the parameter A to vary with rotational state, particularly for the low rotational states where we believe that the adsorption is more sensitive to these stereodynamic effects. That A is independent of J and that $E_0(v,J)$ is highly dependent on J leads us to conclude that the latter description applies to this system. That is, there is a distribution of effective translational barriers associated with different orientations of the molecular axis relative to the surface. Molecules approaching the surface in low rotational states may experience a reorienting torque close to the surface to direct them along the lowest energy path to adsorption. The more rapidly the molecules are rotating, the less likely they will be to follow this path. This type of dynamical effect has been observed in trajectory calculations for the dissociative adsorption of H_2 on Ni.[98,99] For the H_2/Cu system, on the other hand, trajectory calculations for low rotational states have indicated that rotation has little effect on the dissociation probability.[24]

As with the gas-phase model, at high enough J this stereodynamic effect may give way to the "energy" effect in which rotational motion couples to the reaction coordinate allowing rotational energy to be used to surmount the barrier. Coupling of rotation to vibration or translation will enable rotational energy to be channeled into the reaction coordinate, and the effective translational barrier should decrease with increasing J. Such an effect is evident for high J for which $E_0(v,J)$ decreases with increasing J (see Fig. 8). Although the steric effect described above could cause $E_0(v,J)$ to increase linearly with J, the energy effect would cause $E_0(v,J)$ to decrease roughly with J^2. The curves in Fig. 8 represent fits with a quadratic equation, which fits the data well, yielding positive coefficients for the linear terms and negative coefficients for the second-order terms as would be expected for the model described. This system thus exhibits behavior that would be expected if rotational motion couples to the reaction coordinate either through translation or vibration. A prediction of this type of behavior has been made for the corresponding gas-phase model,[58] as well as for the chemisorption of H_2 on Ni(100).[100] Calculations of Gelb and Cardillo for the H_2/Cu system also predict that rotation should enhance adsorption, but these calculations show that enhancement may be the result of an increase in the reactive collision time caused by rotation. During this time the molecule has an opportunity to find a lower energy pathway to dissociation. More recent calculations performed by Yang and Rahman[101] have suggested that rotation couples to both vibration and translation. Calculations of Chang and Holloway,[24,93] however, have indicated that the coupling of rotation to vibration is weak. Although Chang and Holloway have found moderate coupling of rotation to translation, they have also found that this coupling is not sufficient to lead to rotational effects in adsorption.

It has also been suggested that the enhanced reactivity with increasing J for high rotational states observed for gas-phase reactions may be partially attributed to the J-dependent increase in the bond length resulting from centrifugal distortion, which could have an effect similar to that of increased vibrational energy.[28,102] For $J=14$ the bond length increases by $\sim 4\%$ over that of $J=0$. This increase is comparable to the change in equilibrium bond length accompanying an increase in vibration from $v=0$ to $v=2$, which requires the same amount of internal energy as increasing rotation from $J=0$ to $J=14$. The transition state for the dissociation of H_2 on copper, however, is estimated to have a bond length that is 30% larger than the gas-phase bond length,[8] and it is unlikely that a 4% increase in the bond length caused by centrifugal distortion would be sufficient to couple rotational motion to either the vibrational or translational coordinate in the saddle point region of the potential energy surface.

Jacobs and Zare[103] have shown that multiple-bounce interactions with the surface may play a significant role in coupling rotational motion to the reaction coordinate for the trapping of NO on Pt(111). It is unlikely that such a mechanism applies to the present system, however. The depth of the physisorption well for H_2/Cu (0.02 eV) (Refs. 104, 105) is much smaller than the ~ 1 eV well[106] responsible for trapping NO on Pt, and the probability of adsorption into this state becomes insignificant above ~ 0.08 eV, well below the energies required for dissociative chemisorption.[107] Dissipating incidence kinetic energy to the surface[108] or transferring it to internal modes of the

molecule[5] is too inefficient to allow the molecule to release the energy necessary to become trapped. A molecule with 0.6 eV of incidence kinetic energy would need to lose over 96% of this energy in a single collision in order to return to the surface for a second "bounce." It is thus generally accepted that the adsorption of H_2 occurs in a single collision with the copper surface.

B. The effect of vibration on adsorption

The trend of decreasing threshold with increasing vibrational state is easier to understand than the trends observed with the rotational state. This vibrational trend has been observed and explained previously[9–12,17–26] in terms of an extension of the intramolecular bond in the transition state to adsorption. The barrier to adsorption is probably located toward the exit channel of the two-dimensional potential energy surface describing the vibrational and translational degrees of freedom, making coupling of vibrational motion to the reaction coordinate efficient.

The difference between the relative values of $A(v)$ for the different vibrational states, however, is not accounted for by the above explanation. The value of $A(1)$ appears to be anomalously large relative to those of $A(0)$ and $A(2)$. It could be argued that increased stretching of the molecular bond with increased vibrational state reduces steric constraints and thereby promotes adsorption. This effect might explain why $A(1)$ is larger than $A(0)$, but it cannot explain why $A(2)$ is less than $A(1)$. Such behavior is likely to be the consequence of steric factors, but the exact nature of these effects is difficult to imagine with our current level of information.

C. Relative efficacies of translation, vibration, and rotation

To understand the details of the dynamics of adsorption, it is helpful to compare how effectively the various forms of energy promote adsorption. Knowing the translational thresholds to adsorption for each rovibrational state, the relative efficacies of translational, vibrational, and rotational energy are not difficult to establish. For example, if vibrational energy were ineffective in promoting adsorption, the translational threshold for $J=0$ of $v=0$ and 1 would be expected to be the same. If vibrational energy were as effective as translational energy, the translational thresholds for $J=0$ of $v=0$ and $v=1$ would be expected to be separated by 0.371 eV, i.e., by the difference in vibrational energy between the two states. We define the vibrational efficacy to be

$$\mathscr{E}_v=\frac{E_0[(v-1),J=0]-E_0[v,J=0]}{E_v[v,J=0]-E_v[(v-1),J=0]}=\frac{\Delta E_0}{\Delta E_v}, \tag{5}$$

where $E_0[v,J=0]$ and $E_0[(v-1),J=0]$ are the translational thresholds for $J=0$ of vibrational states v and $(v-1)$, and $E_v[v,J=0]$ and $E_v[(v-1),J=0]$ are the internal state energies of the same two states. Thus, if vibrational energy is not effective, $\mathscr{E}_v=0$. If vibrational energy is as effective as translational energy, $\mathscr{E}_v=1$, and if vibration is more effective than translation, $\mathscr{E}_v>1$. We find that $\mathscr{E}_v=0.54\pm0.02$ for both $v=1$ and $v=2$, indicating that translational energy is approximately two times more effective than vibrational energy in promoting adsorption when the incident molecule is not rotating.

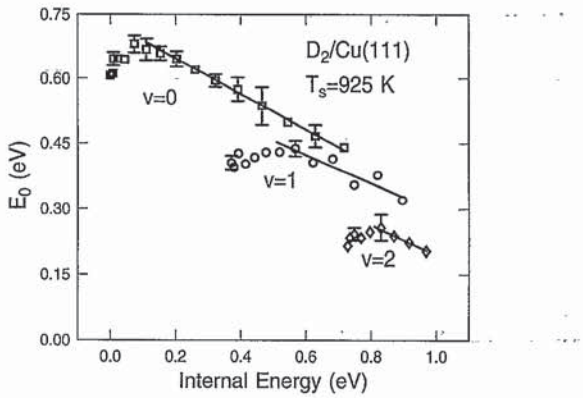

FIG. 13. Dependence of the translational threshold on v and J. Values of the translational threshold, E_0, obtained from fits of Eq. (2) to D_2 time-of-flight distributions for different rovibrational states are plotted against internal (rotational+vibrational) energy. The lines represent linear fits to the points for high rotational states, the slopes of which yield the rotational efficacies for each vibrational state.

The rotational efficacy $\mathscr{E}_r$ is defined similarly to $\mathscr{E}_v$ although its determination and meaning are slightly more complex. Since rotation causes an increase in E_0 for $J<5$, $\mathscr{E}_r$ is negative at low J. The trend is reversed for high J, and $\mathscr{E}_r$ is positive. We calculated $\mathscr{E}_r$ in the high-J limit since it is only at high J that the rotational coupling to the reaction coordinate appears to have a significant influence on the reaction probability. To do so, we plotted E_0 against internal energy and fit a straight line to the points for which $J\geqslant7$ for $v=0$ and $v=1$ and $J\geqslant6$ for $v=2$ (see Fig. 13). The slope of this line gives the rotational efficacy in the limit of high J. We obtained values of $\mathscr{E}_r(v=0)=0.41\pm0.02$, $\mathscr{E}_r(v=1)=0.32\pm0.06$, and $\mathscr{E}_r(v=2)=0.36\pm0.10$. Even for high rotational states, the translational energy is 2.5–3 times more effective than the rotational energy, and the vibrational energy is approximately 30%–70% more effective than the rotational energy. The displacement of the curves for different vibrational states in Fig. 13 also demonstrates that the vibrational energy is more effective than the rotational energy. If, for instance, vibration and rotation were equally effective, the curves would coincide in the (internal) energy range where they overlap.

These results also demonstrate that the observed rotational trends do not change significantly with vibrational state. For high J the rotational efficacy is nearly the same for $v=0$, 1, and 2. In addition, the low J effect might be expected to cause $E_0(v,J)$ to increase linearly with J.[58] Performing linear fits to the first few rotational states shown in Fig. 8 gives slopes that are the same within experimental uncertainty for each vibrational state. Thus, although it appears, from rotational distributions and mean kinetic energies, that the rotational effects diminish with increasing vibration, the dependence of E_0 on v and J

shows that these effects are not substantially less pronounced with increasing v. The reason that the rotational trends appear to depend on v for the rotational distributions and mean energies is related to the fact that these distributions are determined by the overlap of the Maxwell–Boltzmann distribution with the adsorption probability. Higher v will have enhanced overlap with the Maxwell–Boltzmann distribution since these states will have higher adsorption probability at lower kinetic energy. This enhanced overlap with the thermal distribution reduces the observed rotational effects. The value of E_0, on the other hand, is determined by separating the adsorption function from the thermal distribution and thus provides a more direct means for understanding the adsorption dynamics.

V. CONCLUSIONS

We have measured the TOF distributions of 37 rovibrational states of $D_2(v,J)$ desorbed from Cu(111). Strong rotational effects can be seen in the rotational distributions, particularly for $v=0$, where there is greater enhancement of population over the Boltzmann distribution with decreasing J for low J and with increasing J for high J. According to detailed balance the deviations of the rotational distributions from a thermal distribution suggest that the adsorption probability decreases with increasing J for low J and increases with increasing J for high J. This trend is less pronounced with increasing vibrational state; for $v=2$ the rotational distribution does not differ significantly from the Boltzmann distribution.

These strong rotational trends are also observed in the mean translational energies of molecules desorbed into different rotational states. The mean energies increase with increasing J for low J reaching a maximum at $J=5$ and then decrease with increasing J for higher J, especially for $v=0$ and to a lesser extent for $v=1$. Qualitative arguments based on detailed balance lead to the conclusion that the amount of translational energy required for adsorption must depend on the rotational state and must increase with increasing J for $J<5$ and decrease with increasing J for $J>5$. This result is quantitatively confirmed by using detailed balance to establish (for each internal state) $S_0(E_n,v,J)$, the function that describes how the adsorption probability for a single rovibrational state varies with translational energy. The J dependence of the translational threshold or effective barrier is similar to that observed for the mean translational energy, increasing with increasing J from $J=0$, reaching a maximum at $J=5$, and then decreasing. This behavior provides a firm basis for the conclusion that rotational motion hinders adsorption for $J<5$ and enhances it for $J>5$. In contrast to the rotational distributions and the mean energies, in which the rotational trends are less apparent with increasing v, the behavior of $E_0(v,J)$, demonstrates that these rotational trends are *not* less pronounced with increasing vibrational state. This point is made particularly clear by the fact that the rotational efficacy does not change significantly with the vibrational state.

The dependence of the adsorption on the vibrational state is also striking and confirms conclusions drawn from previous studies[9,11,12,17,20–26,67] that vibration is very effective in promoting adsorption. As shown previously, the effective barrier to adsorption decreases with increasing vibrational state. Vibrational motion is along the reaction coordinate to dissociation, and thus vibrational energy is efficiently used to effect adsorption. The desorption TOF measurements, in addition, show that the parameter A, the saturation value of $S_0(E_n)$, depends on the vibrational state and is largest for $v=1$. This parameter appears to be independent of the rotational state.

Although vibrational and rotational motion couple to the reaction coordinate, translational energy is by far the most effective in assisting the molecule over the barrier to adsorption. Translational energy is almost 2 times more effective than vibrational energy and 2.5–3 times more effective than rotational energy in promoting adsorption.

ACKNOWLEDGMENTS

We are grateful to Glenn Kubiak and Greg Sitz for having built the permeation source. We thank Stephen Holloway for helpful discussions and the U.S. Office of Naval Research for partial support under Grant No. N00014-91-J-1023.

[1] R. B. Bernstein, *Chemical Dynamics via Molecular Beam and Laser Techniques* (Oxford University, New York, 1982).
[2] R. D. Levine and R. B. Bernstein, *Molecular Dynamics and Chemical Reactivity* (Oxford University, New York, 1987).
[3] G. Ehrlich, in *Chemistry and Physics of Solid Surfaces VII*, edited by R. Vanselow and R. Howe (Springer-Verlag, Berlin, 1988).
[4] C. T. Rettner and M. N. R. Ashfold, *Dynamics of Gas-Surface Collisions* (Royal Society of Chemistry, Cambridge, 1991).
[5] S. Holloway, in *Dynamics of Gas-Surface Collisions*, edited by C. T. Rettner and M. N. R. Ashfold (Royal Society of Chemistry, Cambridge, 1991).
[6] B. E. Hayden, in *Dynamics of Gas-Surface Interactions*, edited by C. T. Rettner and M. N. R. Ashfold (Royal Society of Chemistry, Cambridge, 1991).
[7] H. A. Michelsen, C. T. Rettner, and D. J. Auerbach, in *Surface Reactions*, edited by R. J. Madix (Springer-Verlag, Berlin, 1993).
[8] J. Harris and S. Andersson, Phys. Rev. Lett. **55**, 1583 (1985).
[9] G. Anger, A. Winkler, and K. D. Rendulic, Surf. Sci. **220**, 1 (1989).
[10] B. E. Hayden and C. L. A. Lamont, Phys. Rev. Lett. **63**, 1823 (1989).
[11] B. E. Hayden and C. L. A. Lamont, Surf. Sci. **243**, 31 (1991).
[12] C. T. Rettner, D. J. Auerbach, and H. A. Michelsen, Phys. Rev. Lett. **68**, 1164 (1992).
[13] M. Balooch, M. J. Cardillo, D. R. Miller, and R. E. Stickney, Surf. Sci. **46**, 358 (1974).
[14] M. Balooch and R. E. Stickney, Surf. Sci. **44**, 310 (1974).
[15] G. Comsa and R. David, Surf. Sci. **117**, 77 (1982).
[16] C. T. Rettner, H. A. Michelsen, D. J. Auerbach, and C. B. Mullins, J. Chem. Phys. **94**, 7499 (1991).
[17] H. A. Michelsen and D. J. Auerbach, J. Chem. Phys. **94**, 7502 (1991).
[18] H. A. Michelsen, C. T. Rettner, and D. J. Auerbach, Phys. Rev. Lett. **69**, 2678 (1992).
[19] D. J. Auerbach, C. T. Rettner, and H. A. Michelsen, Surf. Sci. **283**, 1 (1993).
[20] J. Harris, S. Holloway, T. S. Rahman, and K. Yang, J. Chem. Phys. **89**, 4427 (1988).
[21] J. Harris, Surf. Sci. **221**, 335 (1989).
[22] M. R. Hand and S. Holloway, J. Chem. Phys. **91**, 7209 (1989).
[23] J. K. Nørskov, J. Chem. Phys. **90**, 7461 (1989).
[24] S. Holloway, J. Phys. Condens. Matter **3**, S43 (1991).
[25] D. Halstead and S. Holloway, J. Chem. Phys. **93**, 2859 (1990).
[26] S. Küchenhoff, W. Brenig, and Y. Chiba, Surf. Sci. **245**, 389 (1991).

[27] G. D. Kubiak, G. O. Sitz, and R. N. Zare, J. Chem. Phys. **83**, 2538 (1985).
[28] N. Sathyamurthy, Chem. Rev. **83**, 601 (1983).
[29] R. Altkorn, F. E. Bartoszek, J. deHaven, G. Hancock, D. S. Perry, and R. N. Zare, Chem. Phys. Lett. **98**, 212 (1983).
[30] D. J. Rakestraw, K. G. McKendrick, and R. N. Zare, J. Chem. Phys. **87**, 7341 (1987).
[31] R. Zhang, D. J. Rakestraw, K. G. McKendrick, and R. N. Zare, J. Chem. Phys. **89**, 6283 (1988).
[32] K.-D. Rinnen, D. A. V. Kliner, and R. N. Zare, J. Chem. Phys. **91**, 7514 (1989).
[33] D. A. V. Kliner, D. E. Adelman, and R. N. Zare, J. Chem. Phys. **94**, 1069 (1991).
[34] D. A. V. Kliner, D. E. Adelman, and R. N. Zare, J. Chem. Phys. **95**, 1648 (1991).
[35] R. Zhang, W. J. van der Zande, M. J. Bronikowski, and R. N. Zare, J. Chem. Phys. **94**, 2704 (1991).
[36] A. M. G. Ding, L. J. Kirsch, D. S. Perry, J. C. Polanyi, and J. L. Schreiber, Faraday Discuss. Chem. Soc. **55**, 252 (1973).
[37] F. S. Klein and A. Persky, J. Chem. Phys. **61**, 2472 (1974).
[38] B. A. Blackwell, J. C. Polanyi, and J. J. Sloan, Chem. Phys. **30**, 299 (1978).
[39] H. H. Dispert, M. W. Geis, and P. R. Brooks, J. Chem. Phys. **70**, 5317 (1979).
[40] C.-K. Man and R. C. Estler, J. Chem. Phys. **75**, 2779 (1981).
[41] F. Heismann and H. J. Loesch, Chem. Phys. **64**, 43 (1982).
[42] M. Karplus, R. N. Porter, and R. D. Sharma, J. Chem. Phys. **43**, 3259 (1965).
[43] J. T. Muckerman, J. Chem. Phys. **54**, 1155 (1971).
[44] G. C. Schatz and A. Kupperman, J. Chem. Phys. **65**, 4668 (1976).
[45] A. Persky, J. Chem. Phys. **66**, 2932 (1977).
[46] A. Persky, J. Chem. Phys. **68**, 2411 (1978).
[47] G.-D. Barg, H. R. Mayne, and J. P. Toennies, J. Chem. Phys. **74**, 1017 (1981).
[48] H. R. Mayne and J. P. Toennies, J. Chem. Phys. **75**, 93 (1981).
[49] J. N. L. Connor, W. Jakubetz, A. Lagaña, J. Manz, and J. C. Whitehead, Chem. Phys. **65**, 29 (1982).
[50] H. R. Mayne and C. A. Boonenberg, Chem. Phys. Lett. **108**, 67 (1984).
[51] A. Persky and M. Broida, J. Chem. Phys. **81**, 4352 (1984).
[52] H. J. Loesch, Chem. Phys. **104**, 213 (1986).
[53] H. R. Mayne, Chem. Phys. Lett. **130**, 249 (1986).
[54] H. Kornweitz, A. Persky, and R. D. Levine, Chem. Phys. Lett. **128**, 443 (1986).
[55] H. R. Mayne and S. K. Minick, J. Phys. Chem. **91**, 1400 (1987).
[56] H. J. Loesch, Chem. Phys. **112**, 85 (1987).
[57] N. Sathyamurthy and J. P. Toennies, Chem. Phys. Lett. **143**, 323 (1988).
[58] J. A. Harrison, L. J. Isakson, and H. R. Mayne, J. Chem. Phys. **91**, 6906 (1989).
[59] F. J. Aoiz, V. J. Herrero, and V. Sáez, Chem. Phys. Lett. **161**, 270 (1989).
[60] A. G. Ureña, M. Menéndez, A. S. Sabaté, and A. A. Navarro, Chem. Phys. Lett. **176**, 315 (1991).
[61] A. E. DePristo and A. Kara, Adv. Chem. Phys. **77**, 163 (1990).
[62] M. P. D'Evelyn, A. V. Hamza, G. E. Gdowski, and R. J. Madix, Surf. Sci. **167**, 451 (1986).
[63] M. B. Lee, Q. Y. Yang, and S. T. Ceyer, J. Chem. Phys. **87**, 2724 (1987).
[64] C. T. Rettner and H. Stein, J. Chem. Phys. **87**, 770 (1987).
[65] C. T. Rettner, H. E. Pfnür, H. Stein, and D. J. Auerbach, J. Vac. Sci. Technol. **6**, 899 (1988).
[66] A. C. Luntz and D. S. Bethune, J. Chem. Phys. **90**, 1274 (1989).
[67] B. E. Hayden and C. L. A. Lamont, Chem. Phys. Lett. **160**, 331 (1989).
[68] L. Schröter, G. Ahlers, H. Zacharias, and R. David, J. Electron Spectrosc. Relat. Phenom. **45**, 403 (1987).
[69] L. Schröter, R. David, and H. Zacharias, Surf. Sci. **258**, 259 (1991).
[70] K. W. Kolasinski, S. F. Shane, and R. N. Zare, J. Chem. Phys. **95**, 5482 (1991).
[71] K. W. Kolasinski, S. F. Shane, and R. N. Zare, J. Chem. Phys. **96**, 3995 (1992).
[72] S. F. Shane, K. W. Kolasinski, and R. N. Zare, J. Chem. Phys. **97**, 1520 (1992).
[73] H. Zacharias, Int. J. Mod. Phys. B **4**, 45 (1990).
[74] L. Schröter, Ch. Trame, R. David, and H. Zacharias, Surf. Sci. **272**, 229 (1992).
[75] We estimate that the crystal was $\sim 2°$ misaligned as received.
[76] G. D. Kubiak, Ph.D. thesis, Stanford University, 1985.
[77] E. E. Marinero, C. T. Rettner, and R. N. Zare, Phys. Rev. Lett. **48**, 1323 (1982).
[78] J. Häger, Y. R. Shen, and H. Walther, Phys. Rev. A **31**, 1962 (1985).
[79] More information about the principle of detailed balance can be found in a review written by G. Comsa and R. David (Ref. 85).
[80] G. Comsa, J. Chem. Phys. **48**, 3235 (1968).
[81] W. Van Willigen, Phys. Lett. **28A**, 80, (1968).
[82] R. L. Palmer, J. N. Smith, Jr., H. Saltsburg, and D. R. O'Keefe, J. Chem. Phys. **53**, 1666 (1970).
[83] R. L. Palmer and D. R. O'Keefe, Appl. Phys. Lett. **16**, 529 (1970).
[84] M. J. Cardillo, M. Balooch, and R. E. Stickney, Surf. Sci. **50**, 263 (1975).
[85] G. Comsa and R. David, Surf. Sci. Rep. **5**, 145 (1985).
[86] H.-P. Steinrück, K. D. Rendulic, and A. Winkler, Surf. Sci. **154**, 99 (1985).
[87] E. W. Kuipers, M. G. Tenner, M. E. M. Spruit, and A. W. Kleyn, Surf. Sci. **205**, 241 (1988).
[88] C. T. Rettner, E. K. Schweizer, and C. B. Mullins, J. Chem. Phys. **90**, 3800 (1989).
[89] T. B. Grimley and S. Holloway, Chem. Phys. Lett. **161**, 163 (1989).
[90] H. A. Michelsen, C. T. Rettner, and D. J. Auerbach, Surf. Sci. **272**, 65 (1992).
[91] A. Gelb and M. Cardillo, Surf. Sci. **59**, 128 (1976).
[92] P. Madhaven and J. L. Whitten, J. Chem. Phys. **77**, 2673 (1982).
[93] X. Y. Chang and S. Holloway, Surf. Sci. **251**, 935 (1991).
[94] P. K. Johansson, Surf. Sci. **104**, 510 (1981).
[95] B. A. Hodgson and J. C. Polanyi, J. Chem. Phys. **55**, 4745 (1971).
[96] J. C. Polanyi and J. L. Schreiber, Faraday Discuss. Chem. Soc. **62**, 267 (1977).
[97] J. C. Polanyi and J. P. Toennies, Chem. Phys. **33**, 287 (1978).
[98] A. Cruz and B. Jackson, J. Chem. Phys. **94**, 5715 (1991).
[99] C. Y. Lee and A. E. DePristo, J. Chem. Phys. **87**, 1401 (1987).
[100] J. N. Beauregard and H. R. Mayne (private communication, 1992).
[101] K. Yang and T. S. Rahman, J. Chem. Phys. **93**, 6834 (1990).
[102] W. Grote, M. Hoffmeister, R. Schleysing, H. Zerhau-Dreihöfer, and H. J. Loesch, in *Selectivity in Chemical Reactions*, edited by J. C. Whitehead (Kluwer Academic, Dordecht, 1988).
[103] D. C. Jacobs and R. N. Zare, J. Chem. Phys. **91**, 3196 (1989).
[104] J. Lapujoulade and J. Perreau, Phys. Scri. **T4**, 138 (1983).
[105] U. Harten, J. P. Toennies, and Ch. Wöll, J. Chem. Phys. **85**, 2249 (1986).
[106] C. W. Muhlhausen, L. R. Williams, and J. C. Tully, J. Chem. Phys. **83**, 2594 (1985).
[107] S. Andersson, L. Wilzén, and J. Harris, Phys. Rev. Lett. **55**, 2591 (1985).
[108] M. R. Hand and J. Harris, J. Chem. Phys. **92**, 7610 (1990).